

Small-scale structures in compact steep-spectrum and GHz-peaked-spectrum radio sources

S. Jeyakumar¹, D.J. Saikia¹, A. Pramesh Rao¹, and V. Balasubramanian²

¹ National Centre for Radio Astrophysics, Tata Institute of Fundamental Research, Post Bag No. 3, Ganeshkhind, Pune 411 007, India

² Radio Astronomy Centre, Tata Institute of Fundamental Research, Post Box No. 8, Udhagamandalam 643 001, India

Received 5 October 1999 / Accepted 11 August 2000

Abstract. We determine the small-scale structure for a large sample of Compact Steep Spectrum (CSS) and Gigahertz Peaked Spectrum (GPS) sources and a sample of larger radio sources at 327 MHz using the technique of Inter-Planetary Scintillation (IPS) with the Ooty Radio Telescope. Our observations provide structural information on angular scales ranging from about 50 to a few hundred milliarcsec. We estimate the size and flux density of the scintillating components from the IPS observations. The fraction of flux density of the hotspots estimated from both the IPS observations as well as from interferometric observations for larger sources from the literature exhibits no significant dependence on either the radio luminosity or linear size for the high-luminosity sources. We examine the collimation of radio jets using the sizes of hotspots from both IPS and interferometric observations. The hotspot sizes do not exhibit a significant dependence on the overall linear size for the larger sources, although the CSS and GPS sources were earlier found to evolve in a self-similar way. The IPS observations show evidence of larger-scale structures compared to the known VLBI-scale structures in 8 CSS and GPS radio sources. We discuss the origin of these structures. We also examine the spectra of compact components in GPS sources using both IPS and interferometric measurements, and attempt to distinguish between different processes for explaining their low-frequency spectra.

Key words: galaxies: active – galaxies: jets – galaxies: quasars: general – radio continuum: galaxies

1. Introduction

Compact steep-spectrum sources (CSSs) are defined to be less than about 20 kpc in size ($H_0 = 50 \text{ km s}^{-1} \text{ Mpc}^{-1}$ and $q_0 = 0$), and have a steep high-frequency radio spectrum ($\alpha \geq 0.5$), where $S \propto \nu^{-\alpha}$. This class of objects includes the more compact Gigahertz-Peaked Spectrum (GPS) sources with a turnover in their spectrum at frequencies in the GHz range. The larger CSS sources also sometimes exhibit a flattening or turn-over in the integrated spectrum, but the turnover frequency is usually in the range of a few hundred MHz. High-resolution radio observations of CSS and GPS sources (cf. Fanti et al. 1990; Sanghera et al. 1995 and references therein) reveal a variety of structures

reminiscent of those seen in the more extended sources. The majority of sources have a double-lobed structure, often with a nuclear or core component. Only a small fraction of sources appear to have a highly distorted or complex structure.

A number of possible explanations have been explored to understand the nature of CSS and GPS objects (cf. O’Dea 1998). It has been argued that only a small fraction are likely to appear small because of projection effects (Fanti et al. 1990). Although some may be distorted and confined to small dimensions by a dense interstellar medium in the host galaxy (cf. Wilkinson et al. 1991a,b; Carvalho 1994, 1998), there appears to be a consensus that their small sizes are largely because they are young sources seen at an early stage of their evolution (Carvalho 1985; Fanti et al. 1995; Begelman 1996; Readhead et al. 1996a,b). The GPS sources with a double-lobed structure, the compact doubles (CD), have been proposed to be miniature versions of the classical Fanaroff-Riley class II sources, and have been suggested to evolve from a CD to a CSS and then on to a larger FR II source (Phillips & Mutel 1981; Hodges et al. 1984; Mutel & Phillips 1988; Carvalho 1985).

In this paper we present the results of an Inter-Planetary Scintillation (IPS) study of a large sample of CSS and GPS radio sources at 327 MHz using the Ooty Radio Telescope (ORT). These observations have been made with the objectives of (i) determining the sizes and prominence of hotspots to investigate the collimation of radio jets and the evolution of these sources; (ii) investigating the existence of radio halos at a low frequency on the scale of hundreds of milliarcsec in addition to the more compact structure, suggestive of earlier periods of activity; and (iii) determining the low-frequency spectra of compact components in an attempt to distinguish between different processes to explain the low-frequency turnover in the spectra of GPS sources. We describe the IPS observations, the sample of sources observed by this technique and the results of the IPS observations in Sect. 2. The dependence of the prominence of hotspots from both IPS and interferometric measurements on radio luminosity and linear size, as well as the results on the collimation of radio jets and possible constraints on evolution of radio sources are presented in Sect. 3. The evidence for the existence of possible large-scale structures on the scale of hundreds of mas is presented in Sect. 4. In Sect. 5, we present the spectra of 5 GPS sources where we have attempted to determine the spectra of

the dominant component from IPS and interferometric observations, and discuss possible reasons for their spectral shape.

2. IPS observations

A compact radio source or component seen through the solar wind exhibits scintillations due to electron density fluctuations in the interplanetary medium. The power spectrum of the fluctuations depends on the conditions of the solar wind, and the size and structure of the compact component. Using a suitable model of the solar wind, IPS observations can be used to estimate the angular size of the scintillating component from the power spectrum, and the scintillation index, m , which is defined as $\delta S/S$. Here δS is the rms of the flux density variations and S is the total flux density of the source (e.g. Little & Hewish 1966, 1968; Cohen et al. 1967; Rao et al. 1974). By comparing m_{obs} for a given source with a point source calibrator, m_{cal} , we can estimate μ , the fraction of flux density in the scintillating component. Generally the scintillation index, m , decreases with source size and becomes non-detectable when the source size is so large that the signal to noise ratio is poor. This limits the detectable IPS size to about $0.''4$ at 327 MHz, which we will refer to as the IPS cut-off size. Also for the typical solar wind parameters, and the observing frequency of 327 MHz, the minimum size of the components which can be estimated is about 50 mas (Manoharan & Ananthakrishnan 1990; Gothoskar & Rao 1999). In a typical radio source the compact scintillating components could be the hotspots at the outer edges of the lobes, the nuclear or core components or prominent knots in a jet. If the separation of the compact components, such as the hotspots, is smaller than the IPS cut-off size, the source scintillates as a single source. On the other hand, if the scintillating components in the source are separated by larger than the IPS cut-off size, the components scintillate independently and the parameters estimated from IPS observations are the weighted average values of the different scintillating components.

2.1. The sample of sources

The sample of CSS and GPS sources for the IPS observations have been compiled from a number of papers (Gopal-Krishna et al. 1983; O’Dea et al. 1991; Spoelstra et al. 1985; Savage et al. 1990; Cersosimo et al. 1994; Stanghellini et al. 1990; Peacock & Wall 1982; Sanghera et al. 1995), with the following criteria: (i) declination $|\delta| < 40^\circ$, the normal observable range of the ORT; (ii) total flux density at 327 MHz, $S_{327} > 200$ mJy so that the source can be observed with adequate signal to noise ratio; (iii) the ecliptic latitude of the source is $< 30^\circ$ so that there is enough scintillating power to estimate the parameters reliably. Many sources in our sample occur in more than one of the above lists and they have been counted only once in our list. Also, more recent estimates of sizes and redshifts have led to a number of objects in our sample being larger than the canonical limit of 20 kpc. These have been retained in the list. A few of the sources which were earlier identified as GPS sources appear to have a flat radio spectrum. These have been marked separately in

the table and have not been used in the statistical analyses. Our final sample of largely compact sources consists of 100 objects, 48 of which are GPS sources. In addition, for comparison we have compiled a sample of 19 larger-sized 3C and 4C sources of similar redshift and luminosity. All these sources have $S_{327} > 1$ Jy, and their linear sizes are larger than about 100 kpc for all but one source.

The basic radio and optical properties of the sample of largely CSS and GPS sources and the sample of larger sources are listed in Tables 1 and 2 respectively, which are arranged as follows. Column 1 and 2: IAU name and an alternative name; Column 3: optical identification where G denotes a galaxy, Q a quasar and EF an empty field; Column 4: redshift; Column 5: identification of the object as a GPS source. Some of the sources which were tentatively classified as GPS objects appear to have a flat radio spectrum. These have been indicated as an FSC or flat-spectrum core. Column 6: flux density at 327 MHz in Jy. The flux density values are interpolated from a least-squares fit to the data compiled from the literature, as described in Steppe et al. (1995). A \star denotes an extrapolated value in which a measurement of the flux density was available at about 400 MHz. Column 7: radio luminosity at 5 GHz in units of $\text{W Hz}^{-1} \text{sr}^{-1}$; Column 8: the largest angular size of the source (LAS) in arcsec; for sources with weak extended emission, the LAS is defined by the bright features on opposite sides. Column 9: the projected linear size in kpc; Column 10: structure of radio emission, where T denotes a triple source, MT a misaligned triple where the supplement of the angle formed at the core by the outer hotspots exceed 15° , D a double-lobed one, CJ for a core-jet structure, S for a single component and Cpx for a complex structure. A CJ source is one where there is one dominant component with a jet-like extension rather than a second distinct lobe or hotspot. The double-lobed and triple sources where the flux density ratio of the outer components exceeds 10 are defined to be asymmetric and are identified in this column as AD, AT or AMT. A flat-spectrum core with extended emission on only one-side is indicated by the symbol OS. Any uncertainty in the information or classification is indicated by a question mark. Column 11: references to radio structure. The key to the references are listed in Table 3.

2.2. Observations and analyses

We have observed our sample of sources with the ORT at 327 MHz in the phase-switched mode with a bandwidth of 4 MHz. The intensity variations of a source are sampled at a rate of 20ms. Each source was observed at a number of solar elongations, ϵ , the observations at each elongation lasting about 15–20 minutes. Our observational procedure is similar to the one described by Manoharan & Ananthakrishnan (1990) and Gothoskar & Rao (1999). We also monitored the off source region simultaneously in the total-power mode, to look for any interference, and edited the data accordingly. Since strong scattering occurs when $\epsilon < 12^\circ$, observations were not made for lower values of ϵ . Periods of large solar activity can also modify the average properties of the solar wind and hence the observed power spectrum.

Table 1. Properties of the sample of largely CSS and GPS sources

IAU	Alt.name	ID	z	Sp	S_{327} Jy	P_5 WHz ⁻¹ sr ⁻¹	LAS "	Size kpc	Morph	Ref
0019-000	4C +00.02	G	0.305	GPS	2.6	25.67	0.06	0.36	AD	1,32
0023-263	OB -238	G	0.322		19.3	26.21	0.55	3.42	D	57
0026+346	S4	G	0.600	GPS	1.5*	26.32	0.03	0.266	T	73
0039+230	PKS	EF		GPS	0.5				T?/Cpx	80
0044-056	4C -05.03	Q	1.869		1.8	26.75	1	12.8	D?	62,71,78
0114-211	OC -224	G			11.4		0.6		AT	9,84,85
0121+240	PKS				2.1		2.4		D	81
0127+233	3C 43	Q	1.459		8.4	27.30	2.6	31.5	MT	2,6,28,31
0134+329	3C 48	Q	0.367		44.0	26.52	1	6.76	CJ/Cpx	16,22,31,34,49
0138+136	3C 49	G	0.621		7.6	26.31	0.92	8.28	T	2,28,31
0144+209	PKS	EF		GPS	3.1				-	-
0201+113	OD +101	Q	3.610	GPS	0.3	27.94	3.7	51.2	AD	1,15,32
0218+357	S4	G	0.685	GPS	1.9	26.29	0.36	3.39	See notes	38,39,40
0221+276	3C 67	G	0.310		8.7	25.62	2.47	15	T	2,13,16,28,30,31
0223+341	4C +34.07	Q			3.6*		1.1		T	31,41
0319+121	OE +131	Q	2.662	FSC	2.6	27.85	0.06	0.807	See notes	41,42,86
0320+053	4C +05.14	G	0.575		6.9	26.24	0.03	0.26	S	4,24
0345+337	3C 93.1	G	0.243		6.3	25.30	0.48	2.46	Cpx	30,31,41
0358+004	3C 99	G	0.426		5.4	25.69	4.4	32.5	AT	43,44
0400+258	CTD 026	Q	2.109	GPS	1.3	27.61	5.1	66.5	AD	15,42
0422+178	4C +17.25				2.0		0.76		D	81
0428+205	OF +247	G	0.219	GPS	2.8	25.64	0.21	0.998	T	31,41,66
0445+097	4C +09.17	Q	2.110		2.9	27.27	1.3	16.9	D?	71,78
0457+024	OF +097	Q	2.384	GPS	0.2*	27.95	0.012	0.159	T	80
0500+019	OG +003	Q	1.000	GPS	0.5	27.01	0.015	0.164	T?	1,12,20
0518+165	3C138	Q	0.759		19.8	27.12	0.62	6.1	T	16,28,31,37,46
0528+134	OG +147	Q	2.060	GPS	0.9	27.78	1	13	AD	47,57
0531+194	PKS	G			15.1*		0.5		S	57
0624-058	3C161	Q			51.2		1.3		CJ?	33,55
0658+380	3C173	G	1.035		6.5	26.65	2.46	27.1	D	30,31
0711+356	S4	Q	1.620	GPS	0.6*	27.38	13.5	168	T	38,42,51,52,54
0738+313	OI +363	Q	0.631	FSC	1.0	26.56	66.3	601	T	12,42,86
0740+380	3C186	Q	1.063		7.7	26.49	2.2	24.5	T	28,29,56,58
0741-063	4C -06.18	Q		GPS	10.2				-	-
0742+103	PKS			GPS	1.2		0.012		CJ?	12,15
0743-006	4C -00.28	Q	0.994	GPS	0.3	26.77	0.011	0.12	CJ?	12,15
0751+298	4C +29.27	Q	2.106		1.4	26.86	1.3	16.9	D?	71,78
0752+342	TXS	G			1.2		0.013		S	65
0758+143	3C190	Q	1.970		9.1	27.58	2.6	33.5	MT	16,28,29,33
0802+103	3C191	Q	1.956	GPS	7.9	27.53	4.6	59.2	T	2,33,34,58,78
0843+136	4C +13.39	Q	1.877		1.5	26.82	1.8	23	D	71,78
0848+155	OJ 180	Q	2.007		1.3*	27.12	0.5	6.46	D	71,78
0858+292	3C213.1	G	0.194		5.6	25.05	23.2	101	D	30,31,79
0904+039	PKS			GPS	0.9*				-	-
0914+114	PKS	G		GPS	2.4*				-	-
0941-080	PKS	G	0.228	GPS	3.9	25.37	0.05	0.245	D	11,19
0941+261	OK 270	Q	2.908		2.2*	27.56	1.5	20.4	MT	71,78
1005+077	3C237	G	0.877		19.0	27.07	1.3	13.5	T	16,28,31,33,36
1019+222	3C241	G	1.617		7.6	27.24	0.81	10.1	MT	2,28,30,31,33,36
1045+019	PKS			FSC	0.4		3.1		MT	32,80
1117+146	4C +14.41	G	0.362	GPS	3.7	25.78	0.087	0.583	T	2,60,69,87
1122+195	3C258	G	0.165		2.5	24.62	60	230	D	2,23,30,77
1127-145	PKS	Q	1.187	GPS	5.7	27.53	0.063	0.724	D/CJ?	48,61,63,64
1143-245	PKS	Q	1.950	GPS	0.2	27.60	0.007	0.09	D/CJ?	12,19
1148-171	PKS	Q	1.751	GPS	0.8*	27.23			-	-
1153+317	4C +31.38	Q	0.418		7.2	25.92	0.89	6.5	T	31,35

Table 1. (continued)

IAU	Alt.name	ID	z	Sp	S_{327} Jy	P_5 $\text{WHz}^{-1}\text{sr}^{-1}$	LAS "	Size kpc	Morph	Ref
1210+134	4C +13.46	Q	1.141		2.4	26.72	0.5	5.68	S	78
1221+113	TXS	Q	1.758		1.0*	26.60	1.3	16.4	D/T?	71,78
1237-101	ON -162	Q	0.753	FSC	2.0	26.52	17	167	-	57
1245-197	PKS	Q	1.275	GPS	8.1	27.49	0.3	3.52	AD/CJ?	84
1341+144	4C +14.49				4.5		0.09		D/CJ?	65,81
1345+125	4C +12.50	G	0.120	GPS	7.9	25.19	0.084	0.248	MT?	8,12,63
1354-174	PKS	G	3.147	GPS	0.7*	28.24	0.032	0.438	AD/AMT?	10
1416+067	3C298	Q	1.436		32.9	27.55	1.49	18	T	16,28,30,31,33,78
1433-040	PKS	G		GPS	0.7*				-	-
1442+101	OQ 172	Q	3.522	GPS	1.8	28.47	0.02	0.276	CJ?	3,41
1456+092	OQ 095	Q	1.991		1.8*	27.03	2	25.8	D?	62,78
1518+047	4C +04.51	G	1.296	GPS	2.6	27.45	0.14	1.65	D	15,19,66,67,68
1524-136	PKS	Q	1.687		6.1	27.49	0.538	6.74	MT	9,57,59,84
1543+005	PKS	G	0.550	GPS	2.3*	26.19	0.007	0.0594	T?	80
1548-302	PKS			GPS	1.7*				-	-
1601-222	PKS	G			0.9*				-	-
2008-068	PKS	G		GPS	1.2		0.03		MT?	57,80
2044-027	3C422	Q	0.942		6.8	26.67	1	10.7	AD/Cpx	19,45
2053-201	PKS	G	0.156	GPS	6.5	24.94			-	-
2121-014	PKS			GPS	1.9*				-	-
2126-185	PKS	Q	0.680	GPS	1.0*	26.41			-	-
2128+048	PKS	G	0.990	GPS	3.4	27.13	0.035	0.38	T	1,12,19
2134+004	PKS	Q	1.932	GPS	0.9	28.11	2.8	36	AD	20,21,42,63
2143-156	PKS	Q	0.701		0.6*	26.47			-	-
2146-133	PKS	Q	1.800		5.0	27.32	3.5	44.4	T	71,78
2147+145	PKS				6.5		0.022		D?	27,65,81
2149-306	PKS	Q	2.345	FSC	0.8*	27.59	3	39.7	-	57
2149+056	PKS	G	0.740	GPS	0.2	26.32	0.0035	0.0341	AD?	80
2153-119	PMNJ			GPS	0.5		0.0017		D?	80
2154-183	PKS	Q	1.423	GPS	3.0*	27.23			-	-
2158+101	4C +10.67	Q	1.725		1.7	26.53	0.8	10.1	D?	71,78
2210+016	4C +01.69	G	0.431	GPS	4.3	25.98	0.075	0.558	MT	12,19
2222+051	4C +05.84	Q	2.323		3.2	27.33	3	39.7	T	71,78
2223+210	PKS	Q	1.959	FSC	3.3	27.52	5.3	68.2	T	42,70,78
2230+114	4C +11.69	Q	1.037	FSC	7.5	27.34	2.6	28.7	T	31,53,54,57,69,72
2243-123	PKS	Q	0.630	FSC	1.6*	26.59	3.9	35.3	OS	57
2247+140	4C +14.82	Q	0.237		3.7	25.39	0.2	1.01	D?	31,35
2252+129	3C455	Q	0.543		8.8	26.14	3.12	26.3	D	30,31,78
2322-040	PKS	G		GPS	0.7				-	-
2338+132	4C +13.88				6.5		0.98		D	81
2345-167	PKS	Q	0.576	FSC	1.1*	26.62	3.8	33	-	7,48,57,76
2345+061	4C +06.76	Q	1.546		1.9	26.68	0.98	12	MT/Cpx?	62,78
2353+154	PKS	Q	1.801		2.6	27.10	0.05	0.634	S	78

Notes: 0218+357: This source is gravitationally lensed (O’Dea et al. 1992; Patnaik et al. 1995). The LAS quoted here is the separation between the two lensed images (Polatidis et al. 1995). 0319+121: This spectrum of the source is flat (c.f. Dallacasa et al. 1995; Saikia et al. 1998). The LAS is estimated using the extended emission seen by Murphy et al. (1993).

Data during such periods were also edited since we are primarily interested in the properties of the sources (Manoharan 1993, 1997). For each source, the average power spectrum of the scintillations was obtained at each elongation. From this spectrum, we estimate the scintillation index, m . The typical error in the scintillation index is usually less than about 5 per cent. Variations in the interplanetary medium also leads to a scatter in the

estimated value of μ . The percentage uncertainty in the fraction of scintillating flux density, μ , are listed in Table 4.

An additional source of uncertainty in μ is the scintillations produced by the confusing sources present in the beam. The confusion limit of the ORT is about 1.5 Jy. However, only a fraction of these sources have compact components which are likely to contribute to the scintillations. At low frequencies the scintillating features would be almost entirely the hotspots at the

Table 2. Properties of the sample of larger sources

IAU	Alt.name	ID	z	Sp	S_{327} Jy	P_5 $\text{MHz}^{-1}\text{sr}^{-1}$	LAS "	Size kpc	Morph	Ref
0038-019	4C-02.04	Q	1.690		3.7*	27.15	19.4	243	T	62,78
0109+176	4C+17.09	Q	2.157		2.0*	26.98	13.2	173	MT	62,78
0115+027	4C+02.04	Q	0.672		5.6	26.14	13.1	122	T	74,82
0154+286	3C55	G	0.240		9.5	25.18	69	351	T	14
0222-008	4C-00.12	Q	0.687		2.9	26.03	13.5	127	T	74
0232-042	4C-04.06	Q	1.436		4.5	27.01	13	157	MT	74
0350-073	3C94	Q	0.962		11.9	26.75	41.5	446	D	50
0404+035	3C105	G	0.089		13.1	24.82	335	763	T	18
0736-019	3C185	G	1.033		3.8	26.47	8.9	98.1	D	88
0850+140	3C208	Q	1.110		9.6	26.81	14	158	T	83
0855+285	3C210	G	1.169		7.0	26.79	17.5	200	D	23
0855+143	3C212	Q	1.048		8.8	26.85	10	111	T	5
0941+100	3C226	G	0.823		9.7	26.44	31	315	T	17,75
1012+022	4C+02.30	Q	1.374		2.0	26.52	8.5	102	MT	26
1015+277	4C+27.21	Q	0.469		3.4	25.69	19	148	D	25
1022+194	4C+19.34	Q	0.828		1.3	26.04	44	448	T	74
1023+067	3C243	Q	1.699		4.6	26.88	13.3	167	T	78
1136-135	PKS	Q	0.557		13.4	26.49	15.8	135	T	82

outer edges of the beams in the high-luminosity FR II sources. Estimating the fraction of FR II radio sources in the B2 sample (Allington-Smith 1982) to be about 60 per cent, and assuming the fraction of flux density in the scintillating hotspots to be about 50 per cent, yields a conservative estimate of the scintillation confusion to be about 0.2 Jy. This affects significantly the interpretation of the scintillation visibility μ of the weaker sources. The values for the weak sources with $S_{327} < 0.5$ Jy have been listed in the tables, but have not been used further in the discussions.

The variation of scintillation index, m , with solar elongation for a point source is given by $m \propto (\sin \epsilon)^{-\beta}$. The index β is obtained by a least-squares fit to the observed scintillation index of the IPS calibrator, at various elongations. The compact radio source 1148-001 is the standard IPS calibrator used at the ORT (cf. Venugopal et al. 1985), and observations of this source during 1994-95 have been used to calibrate our observed scintillation indices. The observed scintillation index for a given source can be smaller than the calibrator at the same elongation if either only a fraction μ of the total flux density is in the scintillating component, $m_{obs}(\epsilon) = \mu m_{cal}(\epsilon)$, or the scintillating component is extended. We apply a correction to m_{obs} , for the finite size of the scintillating component using the model of solar wind (Manoharan & Ananthakrishnan 1990; Gothoskar & Rao 1999). This correction could not be applied to 12 of the 91 sources with $S_{327} > 0.5$ Jy in the sample of largely CSS and GPS radio sources (Table 1), and 6 of the 19 larger sources (Table 2) since we could not estimate the size of the component reliably from our observed power spectrum.

The component sizes are estimated from the best fits to the observed power spectrum after trying different values of component sizes and parameters of the standard solar wind model (Manoharan & Ananthakrishnan 1990; Manoharan et al. 1994;

Gothoskar & Rao 1999). The free parameters in this model are the solar wind velocity, random velocity component in the scintillating medium, axial ratio of the irregularities in the medium, the power-law index of the power spectrum of the turbulence of the medium, and the size of the scintillating source. The model fitting was done only for sources observed with a high signal to noise ratio. Even though a 5 mas difference can be distinguished from the power spectrum, the typical inner-scale of the interplanetary medium corresponds to an angular scale of 50 mas, which is the typical error in the estimated angular sizes.

If the structure of the scintillating component is simple, then it might be possible to have an idea of the two-dimensional structure of the source if the direction of the solar wind covers a wide range of position angles across the source. For example, in the case of an elliptical gaussian brightness distribution, a variation of the estimated size from a minimum to a maximum should be observed if the solar wind covers a range of position angles $\geq 90^\circ$ during the different observations of the source. There are 19 sources showing variation of the estimated size with the position angle of the direction of motion of the solar wind. Assuming the structure to be elliptical, we have estimated the parameters of 4 sources where we had enough data to represent the ellipse.

The results of our analyses are presented in Table 4, which is arranged as follows: Column 1: IAU name; Column 2: number of observations used to estimate the size of the scintillating component; Column 3: estimated size of the scintillating component. For the four sources whose two-dimensional structure has been determined assuming it to be elliptical, the major and minor axes and the position angle of the major axis are quoted. The sources which exhibit variation in size, but without enough data to determine the position angle of an elliptical structure unambiguously, the maximum and minimum size are quoted. For the remaining sources, the average size is listed. Column 4:

Table 3. Key to the references for Tables 1 and 2

1	Hodges et al. 1984	31	Spencer et al. 1989	61	Romney et al. 1984
2	Sanghera et al. 1995	32	Stanghellini et al. 1990	62	Lonsdale et al. 1993
3	Gurvits et al. 1994	33	Pearson et al. 1985	63	Fey et al. 1996
4	Broderick & Condon 1975	34	Akujor et al. 1994	64	Bondi et al. 1996
5	Laing pvt. comm.	35	van Breugel et al. 1984	65	Cotton et al. 1989
6	Akujor et al. 1991a	36	Fanti et al. 1985	66	Phillips & Mutel 1981
7	Wardle et al. 1984	37	Fanti et al. 1989	67	Mutel, et al. 1985
8	Shaw et al. 1992	38	Polatidis et al. 1995	68	Mutel & Hodges 1986
9	Mantovani et al. 1998	39	Patnaik et al. 1995	69	Altschuler et al. 1995
10	Frey et al. 1997	40	O'Dea et al. 1992	70	Neff et al. 1989
11	O'Dea & Baum 1997	41	Dallacasa et al. 1995	71	Barthel et al. 1988
12	Stanghellini et al. 1997	42	Murphy et al. 1993	72	Rantakyrö et al. 1996
13	Akujor & Garrington 1995	43	Neff et al. 1995	73	Taylor et al. 1994
14	Fernini et al. 1997	44	Mantovani et al. 1990	74	Hintzen et al. 1983
15	Fey & Charlot 1997	45	Price et al. 1993	75	Bogers et al. 1994
16	Rendong et al. 1991	46	Akujor et al. 1993	76	Preston et al. 1989
17	Jenkins et al. 1977	47	Charlot 1990	77	Bedford et al. 1981
18	Hardcastle et al. 1998	48	Wehrle et al. 1992	78	Barthel & Miley 1988
19	Dallacasa et al. 1998	49	Wilkinson et al. 1991a	79	Gregorini et al. 1988
20	Stanghellini et al. 1998b	50	Miley & Hartsuijker 1978	80	Stanghellini et al. 1999
21	Stanghellini et al. 1998a	51	Cawthorne et al. 1993a	81	Cotton 1983
22	Wilkinson et al. 1984	52	Cawthorne et al. 1993b	82	Saikia et al. 1989
23	Strom et al. 1990	53	Pearson et al. 1980	83	Bridle et al. 1994
24	Mantovani et al. 1992	54	Pearson & Readhead, 1988	84	Mantovani et al. 1994a
25	Fanti et al. 1977	55	Schilizzi et al. 1982	85	Mantovani et al. 1994b
26	Jackson et al. 1999	56	Saikia et al. 1984	86	Saikia et al. 1998
27	Cotton et al. 1984	57	Perley 1982	87	Bondi et al. 1998
28	van Breugel et al. 1992	58	Cawthorne et al. 1986	88	Saikia et al. in prep.
29	Spencer et al. 1991	59	Mantovani et al. 1988		
30	Akujor et al. 1991b	60	Padrielli et al. 1991		

the total number of IPS observations; Column 5: the fraction of flux density of the scintillating component, μ , and the percentage error in μ .

3. Hotspots in CSS and larger sources

The hotspots, which are the high brightness regions in the outer lobes of the high-luminosity FR II radio sources, indicate the Mach disks where the jets terminate. The hotspots usually subtend small angles in the radio cores suggesting the high degree of collimation of the jets in these sources (Bridle & Perley 1984; Bridle et al. 1994; Fernini et al. 1997). However, the jet momentum may be spread over a larger area than the cross-section of the jet itself due to the dentist-drill effect discussed by Scheuer (1982), where the end of the jet wanders about the leading contact surface drilling into the external medium at slightly different places at different times. Recent simulations of 3D supersonic jets suggest that cocoon turbulence drives the dentist-drill effect (Norman 1996).

In this section we study some of the properties of the hotspots for CSS as well as larger objects using the results from our IPS survey and also available interferometric observations of hotspots. IPS observations enable us to estimate the weighted average of the fraction of flux density in the scintillating components and their sizes. For sources larger than about 400 mas

the scintillating components are usually the hotspots at the outer edges of the lobes. Since the cores in CSSs are usually weak, especially at low frequencies, the scintillating components are the hotspots in the lobes. Over the last few years the sizes of hotspots have also been determined reasonably reliably from interferometric observations for samples of compact steep-spectrum radio sources using largely VLBI and MERLIN observations, as well as for the larger objects using the VLA. Although there is no well-accepted definition of a hotspot (cf. Laing 1989; Perley 1989), we have used the following empirical definition. The hotspots are defined to be the brightest features in the lobes located further from the nucleus than the end of any jet, and in the presence of more extended diffuse emission these should be brighter by at least a factor of 4 (cf. Bridle et al. 1994). In the presence of multiple hotspots, only the primary hotspot has been considered.

In the following subsections we consider the possible dependence of the fraction of flux density from the hotspot and its size on both radio luminosity and overall projected linear size, and discuss possible constraints these might place on models of evolution of radio sources. We have excluded sources with prominent flat-spectrum nuclei, and those with a complex or core-jet morphology, and have considered only those sources where the scintillations are likely to be produced by the hotspots in the

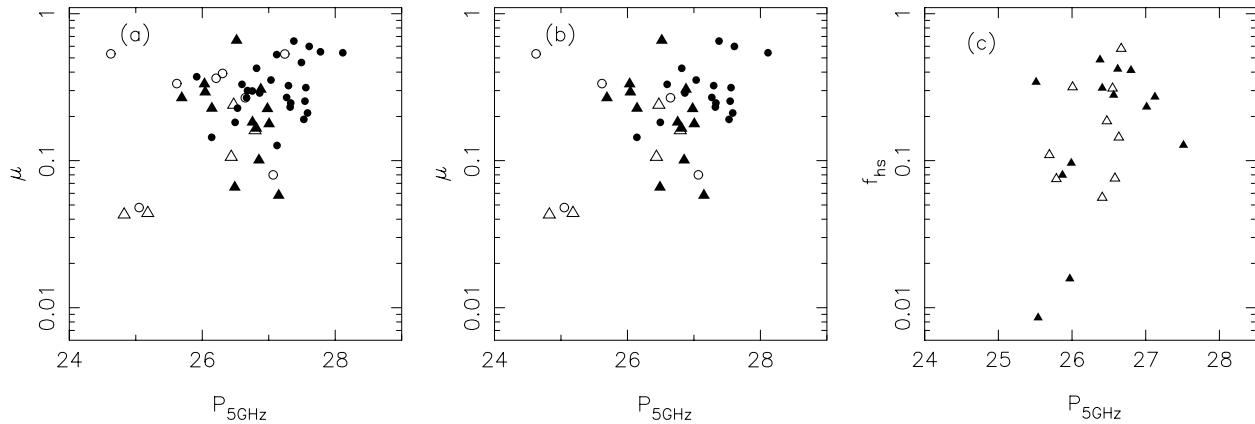


Fig. 1a–c. The scintillation visibility, μ for sources **a** with $LAS > 400$ mas, **b** $LAS > 1$ arcsec and **c** the fraction of emission from the hotspots, f_{hs} , estimated from interferometric observations by B94 and F97 are plotted against the total radio luminosity at 5 GHz. The sample of largely CSS and GPS sources (Table 1) are shown by open and filled circles for galaxies and quasars respectively, while the larger galaxies and quasars (Table 2, B94 and F97) are shown by open and filled triangles respectively.

outer lobes. In the GPS sources with two outer components, we have assumed that these features are likely to be hotspots rather than being the counterparts of flat-spectrum nuclei. The compact-double structures seen in several GPS sources, lack of variability, and polarization measurements as in 2134+004 (cf. Stanghellini et al. 1998b) lend some support to such an interpretation.

3.1. Hotspot prominence and radio luminosity

The dependence of the prominence of the hotspots on radio luminosity was examined about 20 years ago (e.g. Jenkins & McEllin 1977; Kapahi 1978). Jenkins & McEllin reported a strong correlation of the prominence of the hotspots with radio luminosity for the well-studied sample of 3CR radio sources. They defined the hotspots to be features with a size less than about 15 kpc. Kapahi (1978) argued that this correlation is possibly due to the effective resolution being coarser for the higher redshift and hence higher luminosity sources. We investigate this relationship for the CSS as well as larger objects using both the IPS and interferometric measurements.

In Figs. 1a and b the scintillation visibility, μ , is plotted against the total radio luminosity at 5 GHz for the sources from our IPS observations (Tables 4 and 5) with an $LAS > 400$ and 1000 mas respectively. Since the effective size of the hotspots estimated from IPS observations can depend on the relative prominence of the compact and halo components as well as their separation (cf. Duffet-Smith 1980), we have examined these trends for sources > 1000 mas where the blending of the two oppositely-directed hotspots is minimal. The scintillation visibility, μ , ranges from about 0.04 to 0.7 with most objects in the range of ~ 0.1 to 0.7. The median value of μ is about 0.3. The luminosity of most objects at 5 GHz lie in the range of about $10^{25.5}$ to 10^{28} $\text{W Hz}^{-1} \text{sr}^{-1}$, and in further discussions in this paper we confine ourselves largely to objects in this luminosity range. The scintillation visibility μ - luminosity diagrams for all the sources in Tables 1 and 2 with $S_{327} > 0.5$ Jy (Figs. 1a

and b), show no evidence of a significant dependence on radio luminosity.

We have also examined this relationship using the hotspot flux densities listed by Bridle et al. (1994, hereinafter referred to as B94) and Fernini et al. (1993, 1997, hereinafter referred to as F97), whose sources have a similar luminosity to those of our samples and have been observed with resolution of about a few hundred mas, which is comparable to our IPS cut-off size. A plot of the fraction of the hotspot flux densities, $f_{hs} = (S_{h1} + S_{h2})/S_{total}$, from the two lobes against the total radio luminosity at 5 GHz for the sources from B94 and F97 are presented in Fig. 1c. The interferometric measurements also do not show a significant dependence of hotspot prominence on radio luminosity.

3.2. Hotspot prominence and linear size

We have presented the μ -linear size diagram for the IPS samples described in the earlier section in Figs. 2a and b, and the f_{hs} -linear size diagram for the B94 and F97 sources in Fig. 2c. The Spearman rank correlation coefficient for the IPS sample of sources with $LAS > 1000$ mas is -0.32 , compared to -0.15 for the B94 and F97 sources. Again, we find no evidence of a significant dependence of either μ or f_{hs} on linear size for these high-luminosity objects. There is, at best, a weak anticorrelation.

A relation between the prominence of hotspots with source size, and the total luminosity can in principle provide constraints on the models of evolution of radio sources. The luminosity of the hotspot depends on the pressure in the hotspot and the size of the hotspot. Many models in the literature assume that the contribution of the hotspot to the total luminosity is negligible (Kaiser et al. 1997; Blundell et al. 1999) or do not consider the evolution of the hotspot independently (Chyzy 1997; Begelman 1996). The self-similar models assume that the pressure in the head of the jet, which is essentially the hotspot, scales with the mean cocoon pressure (Kaiser et al. 1997; Begelman 1996) by

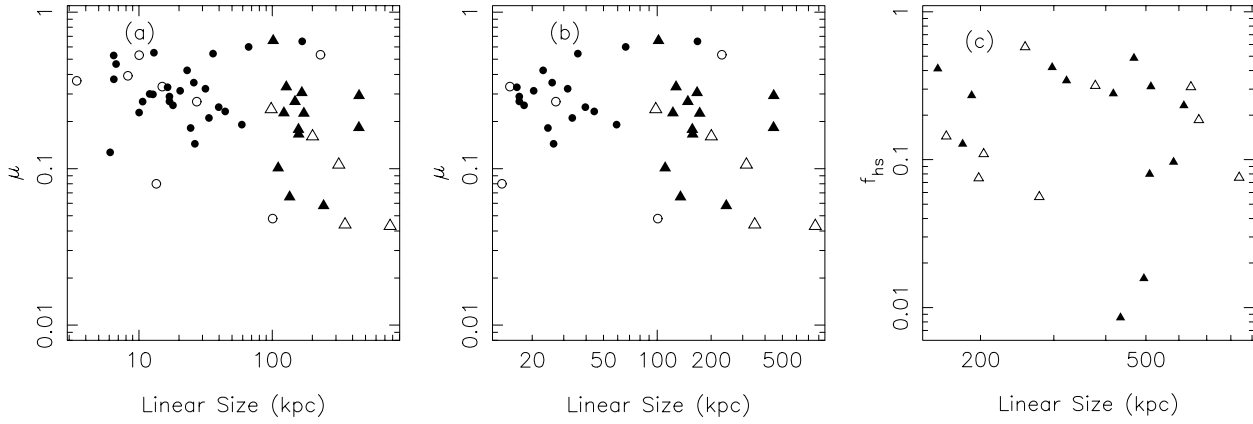


Fig. 2a–c. The scintillation visibility, μ for sources **a** with LAS > 400 mas, **b** LAS > 1 arcsec and **c** the fraction of emission from the hotspots, f_{hs} , estimated from interferometric observations by B94 and F97 are plotted against the projected linear size. The symbols have the same meaning as in Fig. 1.

means of adjusting the size of the working surface. These models predict that the cocoon luminosity decreases as the source ages. This would suggest, in the light of our data, that the hotspot luminosity also decreases as the source grows old. Non-relativistic numerical simulations have been attempted to understand the structures of the hotspots (Wilson & Scheuer 1983; Smith et al. 1985; Norman & Balsara 1993). Although these simulations reveal dynamically varying structures of the hotspots, the luminosity evolution needs to be studied. The simulations involving relativistic electron transport with the 3D MHD simulations of jets (Jones et al. 1999a; Tregillis et al. 1999; Jones et al. 1999b) might provide better insight into the evolution of the hotspots.

3.3. Sizes of hotspots and collimation of radio jets

A study of the variation of the size of the hotspots on the overall linear size of the objects could provide useful clues on the collimation of radio jets. A plot of the size of the scintillating components for sources larger than 1000 mas, against the overall linear size of the source shows no significant dependence of the hotspot size on the overall size of the object (Fig. 3a). To examine any effect of contamination by diffuse emission around the hotspots (cf. Hewish & Readhead 1976; Duffet-Smith 1980) we have confined ourselves to objects above 1000 mas, and have also considered separately objects with $\mu > 0.3$ (Fig. 3b). We again find no evidence of a significant relationship. We also examine this trend using the sizes of hotspots determined by B94 and F97, which have similar luminosity to our IPS sample (Fig. 3c). The interferometric measurements for the B94 and F97 sources also suggest that the hotspot sizes do not exhibit a significant dependence on the overall linear size. The hotspot sizes remain nearly constant with a mean value of about 3 kpc although the hotspot sizes range from about 1 to 10 kpc, implying that the jets have an approximately constant mean width beyond about 20 kpc.

Jeyakumar & Saikia (2000a,b) have earlier examined the dependence of hotspot size on projected linear size for CSS and GPS objects, and find that the hotspot size increases linearly with

the total linear size, suggesting that they evolve in a self-similar way. By comparing this trend with larger objects observed with a similar number of resolution elements, they suggested that there is a flattening of the relationship beyond about 20 kpc. The plots in Fig. 3 where most of the objects are larger than about 10 kpc are consistent with this flattening.

The relationship between the hotspot sizes and the overall size of the source suggest that the jets are largely confined. The jets could be confined by the ambient pressure whose density falls with distance from the nucleus for sources less than about 20 kpc, while for larger scales the jets could be possibly magnetically confined. Numerical simulations of the propagation of jets also show that the hotspot sizes do not tend to increase with linear size as the jets propagate outwards beyond a certain distance (Sanders 1983; Wilson & Falle 1985).

The recollimation of the jet can occur if the jet pressure falls more rapidly than the ambient pressure. In such a scenario one would expect recollimation to occur at a distance where the jet pressure falls below the ambient pressure. In the model of Sanders (1983) applied to the jet in NGC 315, the reconfinement of the jet is accompanied by conical shocks which heat the jet causing it to reexpand. In this scenario, the reconfinement region beyond about 20 kpc, where the mean hotspot width has an approximately constant value of ~ 3 kpc, requires a high ambient pressure, comparable to or larger than the jet pressure, beyond the CSS stage. On the large scales, where the ambient pressure may not be sufficient for confinement, the jet could be possibly held together by its own toroidal magnetic field (cf. Begelman et al. 1984). Magnetic collimation provides a natural explanation of the observed trend of a nearly constant width in the large sources. The mechanism of self-collimation by current-carrying jets has been examined by Appl & Camenzind (1992, 1993a,b), and the development of Kelvin-Helmholtz and current-driven instabilities in these relativistic MHD jets have been studied by Appl (1996). In this scenario, the jet is initially pressure confined and becomes self-collimated by the magnetic pressure when the ambient pressure drops below the jet pressure. The width of the jet in the pressure confined regime is determined

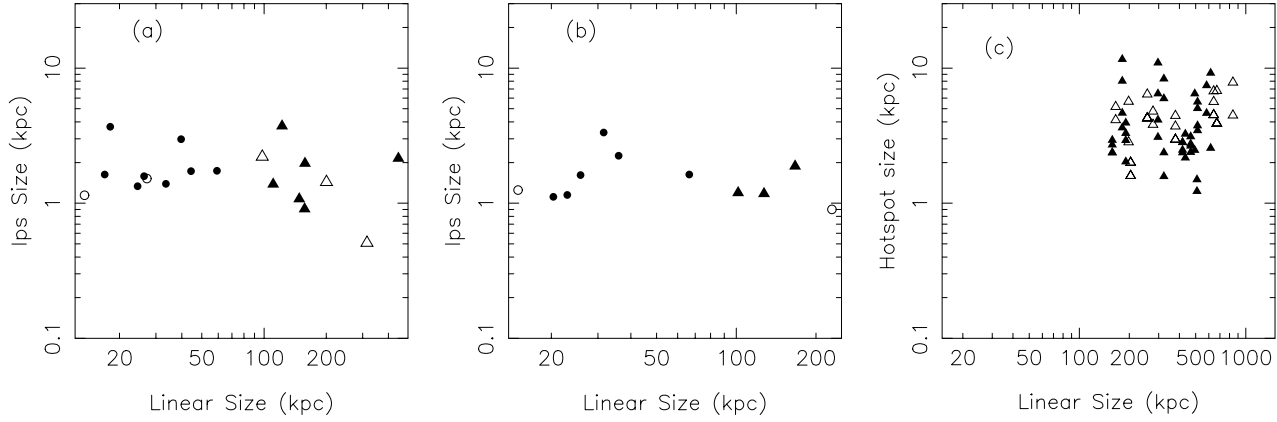


Fig. 3a–c. The linear sizes of the scintillating components for all the objects in Tables 1 and 2 with an LAS > 1 arcsec are plotted against the total projected linear size in panel **a** and for those with $\mu > 0.3$ in panel **b**. In panel **c** the sizes of the hotspots from B94 and F97 are plotted against the projected linear sizes of these objects. The symbols have the same meaning as in Fig. 1.

by the ambient pressure alone, where the jet current is shielded by the surface currents (Appl & Camenzind 1992). The increase in jet width with source size in this phase is due to the decrease in ambient pressure. Self-collimation becomes important when the ambient pressure falls just below the jet pressure. At this point, the current, I , is estimated to be $\approx 10^{17} P^{1/2} R_j$ amp where P is in units of 10^{-12} dyn cm^{-2} and the radius of the jet R_j is in kpc (Appl & Camenzind 1992). For a hotspot radius of 1.5 kpc, which is the mean value for our large sources, and typical jet pressure of $\sim 10^{-10}$ dyn cm^{-2} the current required to be carried by the jet is about 10^{18} amp. The variation of the sizes of the hotspots is consistent with pressure confinement in the CSS phase with the ambient pressure falling with distance from the nucleus, while at larger distances from the nucleus where the ambient pressure has fallen below the jet pressure, the jet could be possibly magnetically confined.

4. Extended emission or milli halos around CSSs

The sources whose overall separation of the components are less than the IPS cut-off size scintillate as a single source. A comparison of the sizes of the scintillating components with the VLBI-scale structure should enable us to infer the existence of milli-halos on the scale of hundreds of milliarcsec which may have been resolved out in the high-frequency VLBI observations, which are usually between 1.4 and 5 GHz. The extended emission with steeper spectrum may also be more prominent at low frequencies.

In Fig. 4, we plot the sizes of the scintillating components inferred from the IPS observations against the largest angular size estimated from the VLBI images for all objects with an overall angular separation less than about 400 mas. There are 21 objects which satisfy this criterion, and their properties can be found in Tables 1 and 2.

The sizes of the scintillating components estimated from the IPS observations tend to be larger than the interferometric measurements, except for the source 0428+205. Here, the IPS size is significantly smaller than the LAS, which is defined by

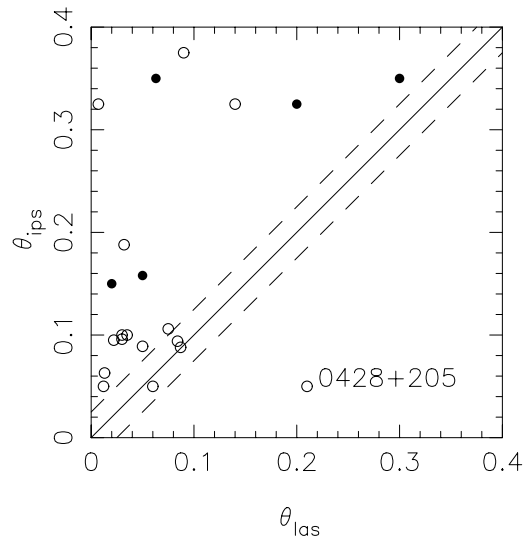


Fig. 4. The size of the scintillating component, θ_{IPS} , is plotted against the LAS estimated from VLBI observations for CSS and GPS sources whose VLBI structure < 400 mas. The symbols are as defined in Fig. 1. The source 0428+205 has been discussed in the text.

the weak extended emission towards the north-west. The peak brightness of this component is about a factor of 37 weaker than the dominant component seen in the VLBI image at $\lambda 18$ cm. The size of the dominant component, whose peak brightness in the VLBI image is 1476 mJy/beam (Dallacasa et al. 1995) and which is likely to contribute to most of the scintillating power, is similar to the IPS size.

Since the uncertainty in the IPS size could be as large as about 50 mas, we identify only those sources whose difference between the IPS and VLBI sizes to be at least about 3 times 50 mas to be strong candidates for milli halos. These include the sources 1127–145, 1341+144, 1354–174, 1518+047 and 1543+005. Those whose difference lies between 2 and 3 times are 1442+101, 2247+140 and 2353+154, and these are possible candidates for millihalos. These 8 sources are described

Table 4. Observed parameters of largely CSS, GPS sources

IAU-name	N_s	$\theta_1 \times \theta_2$ " × "	PA °	N_t	μ
0019–000	3	< 0.050		6	0.87 ± 0.06
0023–263	2	0.162		4	0.36 ± 0.03
0026+346				1	0.38 ± 0.05
0039+230				6	0.88 ± 0.03
0044–056	2	0.125		7	0.30 ± 0.04
0114–211	6	0.350×0.200		6	0.55 ± 0.03
0121+240	6	$0.215 \times < 0.040$	58	10	0.47 ± 0.03
0127+233	7	0.275×0.125		8	0.32 ± 0.04
0134+329	6	0.225		6	0.31 ± 0.03
0138+136	4	0.081		10	0.39 ± 0.03
0144+209				4	0.08 ± 0.03
0201+113				4	0.87 ± 0.06
0218+357				4	0.20 ± 0.03
0221+276	4	0.206		4	0.34 ± 0.06
0223+341	4	0.194		5	0.27 ± 0.03
0319+121	3	< 0.050		4	0.58 ± 0.04
0320+053	2	0.100		6	0.73 ± 0.03
0345+337	6	0.183		6	0.36 ± 0.03
0358+004	7	0.218		7	0.44 ± 0.03
0400+258	1	0.125		3	0.60 ± 0.09
0422+178	2	0.125		2	0.42 ± 0.09
0428+205	2	< 0.050		2	0.54 ± 0.10
0445+097	2	0.125		5	0.27 ± 0.06
0457+024				2	1.12 ± 0.04
0500+019				2	0.77 ± 0.02
0518+165	2	0.112		3	0.13 ± 0.13
0528+134	2	< 0.050		3	0.55 ± 0.02
0531+194	2	0.115		2	0.29 ± 0.05
0624–058	6	0.275×0.200		6	0.22 ± 0.03
0658+380	5	0.138		6	0.27 ± 0.03
0711+356				4	0.65 ± 0.03
0738+313	2	< 0.050		3	0.42 ± 0.02
0740+380	3	0.120		3	0.18 ± 0.03
0741–063	5	0.150×0.075		5	0.54 ± 0.02
0742+103	3	< 0.050		3	0.82 ± 0.06
0743–006				4	1.11 ± 0.05
0751+298				1	0.29 ± 0.05
0752+342	2	0.063		3	0.35 ± 0.04
0758+143	3	0.108		7	0.21 ± 0.04
0802+103	2	0.135		3	0.19 ± 0.05
0843+136	1	0.090		6	0.43 ± 0.03
0848+155	1	< 0.050		4	0.53 ± 0.04
0858+292				8	0.05 ± 0.05
0904+039	1	0.080		9	0.66 ± 0.03
0914+114	3	0.080		5	0.67 ± 0.04
0941–080	6	0.089		8	0.61 ± 0.03
0941+261	4	0.082		6	0.31 ± 0.03
1005+077	2	0.110		4	0.08 ± 0.29
1019+222	2	0.138		3	0.53 ± 0.04
1045+019				4	0.62 ± 0.09
1117+146	6	0.088		8	0.73 ± 0.03
1122+195	9	0.235×0.070	176	12	0.53 ± 0.03
1127–145	15	$0.350 \times < 0.050$		17	0.49 ± 0.04
1143–245				1	0.80 ± 0.05
1148–171				3	0.24 ± 0.14
1153+317	4	0.200×0.105		4	0.37 ± 0.04

Table 4. (continued)

IAU-name	N_s	$\theta_1 \times \theta_2$ " × "	PA °	N_t	μ
1210+134	5	0.300×0.085		14	0.38 ± 0.04
1221+113				9	0.33 ± 0.06
1237–101	2	0.213		10	0.56 ± 0.03
1245–197	9	$0.350 \times < 0.050$		11	0.51 ± 0.03
1341+144	8	$0.375 \times < 0.050$		11	0.51 ± 0.03
1345+125	4	0.094		9	0.59 ± 0.03
1354–174	2	0.188		9	1.10 ± 0.04
1416+067	9	0.305×0.120	112	13	0.25 ± 0.05
1433–040	2	0.133		10	1.00 ± 0.06
1442+101	1	0.150		10	0.67 ± 0.05
1456+092	1	0.125		8	0.35 ± 0.07
1518+047	8	0.325×0.150		11	0.62 ± 0.04
1524–136	5	0.100		8	0.47 ± 0.06
1543+005	8	0.325×0.075		9	0.74 ± 0.04
1601–222	1	< 0.050		3	0.32 ± 0.07
2008–068	6	0.096		10	0.49 ± 0.05
2044–027	14	0.245×0.090	68	14	0.27 ± 0.03
2053–201				3	0.07 ± 0.08
2121–014	8	0.112		11	0.68 ± 0.04
2126–185	1	0.100		4	0.79 ± 0.10
2128+048	10	0.100		10	0.62 ± 0.04
2134+004	9	$0.175 \times < 0.050$		13	0.54 ± 0.03
2143–156	4	0.056		7	1.04 ± 0.05
2146–133	6	0.136		7	0.23 ± 0.05
2147+145	5	0.095		5	0.49 ± 0.03
2149–306	6	0.125×0.075		10	0.57 ± 0.04
2149+056				3	0.69 ± 0.04
2153–119				5	0.76 ± 0.06
2154–183	3	0.108		4	0.61 ± 0.03
2158+101	1	0.100		7	0.23 ± 0.08
2210+016	9	0.106		9	0.72 ± 0.07
2222+051	7	0.225×0.125		7	0.25 ± 0.06
2223+210	3	0.125		3	0.41 ± 0.07
2230+114	3	0.083		5	0.44 ± 0.06
2243–123	4	0.081		7	0.72 ± 0.06
2247+140	6	0.325×0.150		6	0.65 ± 0.04
2252+129	4	0.188		5	0.14 ± 0.04
2322–040	1	0.125		6	0.50 ± 0.03
2338+132	3	0.112		3	0.45 ± 0.03
2345–167	3	0.088		6	1.07 ± 0.03
2345+061				1	0.30 ± 0.05
2353+154	3	0.158		5	0.58 ± 0.04

briefly below. The IPS sizes of the remaining 12 sources with LAS $\lesssim 400$ mas, namely 0019–000, 0320+053, 0742+103, 0752+342, 0941–080, 1117+146, 1245–197, 1345+125, 2008–068, 2128+048, 2147+145 and 2210+016, are consistent with the VLBI sizes.

There appears to be evidence of extended emission around some of the CSSs on scales few times larger than the known size of the sources. We refer to these structures as milli-halos. These low-frequency halos are expected to have steeper radio spectra and could be contributing less to the total flux density at high frequencies; and could also have been resolved out in the

Table 5. Observed parameters of larger sources

IAU-name	N_s	$\theta_1 \times \theta_2$ " × "	PA °	N_t	μ
0038–019				1	0.06 ± 0.05
0109+176				2	0.23 ± 0.04
0115+027	1	0.400		1	0.23 ± 0.05
0154+286				3	0.04 ± 0.03
0222–008	2	0.125		3	0.33 ± 0.04
0232–042	1	0.075		1	0.18 ± 0.05
0350–073	2	0.200		2	0.18 ± 0.04
0404+035				1	0.04 ± 0.05
0736–019	1	0.200		3	0.24 ± 0.08
0850+140	1	0.175		1	0.17 ± 0.05
0855+285	1	0.125		1	0.16 ± 0.05
0855+143	1	0.125		1	0.10 ± 0.05
0941+100	2	< 0.050		2	0.11 ± 0.02
1012+022	1	0.100		2	0.66 ± 0.10
1015+277	2	0.138		2	0.27 ± 0.04
1022+194				2	0.29 ± 0.02
1023+067	1	0.150		1	0.31 ± 0.05
1136–135				1	0.07 ± 0.05

interferometric maps. There is often evidence of missing flux density in the VLBI images, but evidence of these halos from the integrated spectra is difficult to establish because the low-frequency integrated spectra as well as the spectra of individual components are not well-determined. One possible scenario for such structures could be earlier periods of activity which is presently fading out due to radiative and other losses. Another possibility is that the milli-halo is composed of relativistic particles which have diffused out from the jet or the nucleus. Such milli-halos with sizes of the order of about a kpc have been seen in a few nearby AGN from high-resolution and high sensitivity observations (Silver et al. 1998; Carilli et al. 1998). The sizes of extended emission detected in CSSs by IPS observations are in the range of about 250 pc to 4 kpc. These could be similar to the milli-halos seen in the nearby AGNs.

1127–145: This source has a core-jet type of structure at 2.32 GHz with an overall angular size of about 63 mas (Fey et al. 1996). At higher resolution the dominant component is resolved into a double-lobed source with an angular separation between the peaks of emission of about 3.7 mas (Romney et al. 1984; Wehrle et al. 1992; Bondi et al. 1996; Fey et al. 1996). The LAS of the source estimated from the IPS observations is about 350 mas, significantly larger than the known VLBI-scale structure.

1341+144: The source 1341+144 is a possible double with an angular separation between the peaks of emission of about 60 mas (Cotton et al. 1989). The LAS inferred from the IPS observations is about 375 mas.

1354–174: It is a highly asymmetric source where the flux density ratio of the outer components is about 57, and the overall angular size is about 32 mas (Frey et al. 1997). The IPS size of the source is 188 mas.

1442+101: We estimate the size of the scintillating component from IPS observations to be about 150 mas. The VLBI map by Gurvits et al. (1994) shows a core and extension resembling a jet, with the largest separation of the components being ~ 15 mas. The VLBI map at 18 cm by Dallacasa et al. (1995) shows a core and jet-like extension with the core in the northern end, contrary to the Gurvits et al. (1994) image. If the core is towards the south, the possible jet has a very steep spectrum. The LAS of the source from the VLBI image is about 24 mas, while the size estimated from the IPS observations is about 150 mas.

1518+047: Phillips & Mutel (1981) find the source to be double-lobed at 18 cm with an overall LAS of 135 mas. Both the lobes are resolved into two components at 5GHz by Mutel et al. (1985). A recent image by Dallacasa et al. (1998) also shows the double-lobed structure. The IPS size of the source is 325 mas.

1543+005: It is a possible triple source with an overall angular size of 7 mas (Stanghellini et al. 1999). The size of the scintillating component is about 325 mas.

2247+140: MERLIN observations by Spencer et al. (1989) show that it is a single source with an angular size of ~ 200 mas. VLA observation by van Breugel et al. (1984) show that it is resolved into a possible double-lobed source. The IPS size of the source is about 325 mas.

2353+154: Barthel & Miley (1988) found this source to have a single component with an angular size of 50 mas. The IPS size of the source is about 158 mas.

5. Spectra of scintillating components in GPS sources

The spectral turnover of GPS sources at low radio frequencies could be either due to synchrotron self absorption or free-free absorption. In order to try and distinguish between these two principal processes, we attempted to determine better the spectra of the compact component using both IPS observations at low frequencies and VLBI observations at higher frequencies. Since all the emission with compact structures less than about 400 mas would contribute to the scintillating power, we have confined ourselves to those GPS sources in our IPS sample whose emission at a higher frequency is dominated by a single compact component. The peak brightness in any secondary component in the VLBI images is less by at least a factor of about 10, and it is reasonable to assume that the scintillations are almost entirely from the dominant component. Five of the objects in our sample satisfy this criterion.

We present the integrated spectra as well as that of the dominant component from the IPS and VLBI observations in Fig. 5; and the results are summarized in Table 6 which is arranged as follows. Column 1: source name; Column 2: optical identification; Column 3: the redshift; Column 4: frequency of the peak in the integrated spectrum, ν_p^T , in GHz; Column 5: frequency of the peak in the spectrum of the dominant component, ν_p^C , in GHz; Column 6: the flux density of the dominant component at the peak frequency; Columns 7: the range in the VLBI sizes of the prominent components in mas, with each size being the

Table 6. Estimated parameters of 5 GPS sources with one dominant component

Source	Id	z	ν_p^T GHz	ν_p^C GHz	S_p^C Jy	θ_{vlbi}^C mas	θ_{ips}^C mas	θ_{SSA} mas	$n_e \text{ cm}^{-3}$ 10 pc	50 pc
0019-000	G	0.305	0.7	0.8	3.1	< 5.0	< 50	3.35	437	195
0400+258	Q	2.109	1.4	1.5	1.1	0.3 – 2.8	125	1.13	845	378
0428+205	G	0.219	1.0	1.7	3.3	~ 1.7	< 50	1.32	964	431
0711+356	Q	1.620	1.7	1.9	1.6	0.1 – < 6.9	–	0.97	1084	485
0742+103			2.0	2.1	4.6	0.4 – 1.7	< 50	1.36	1204	538

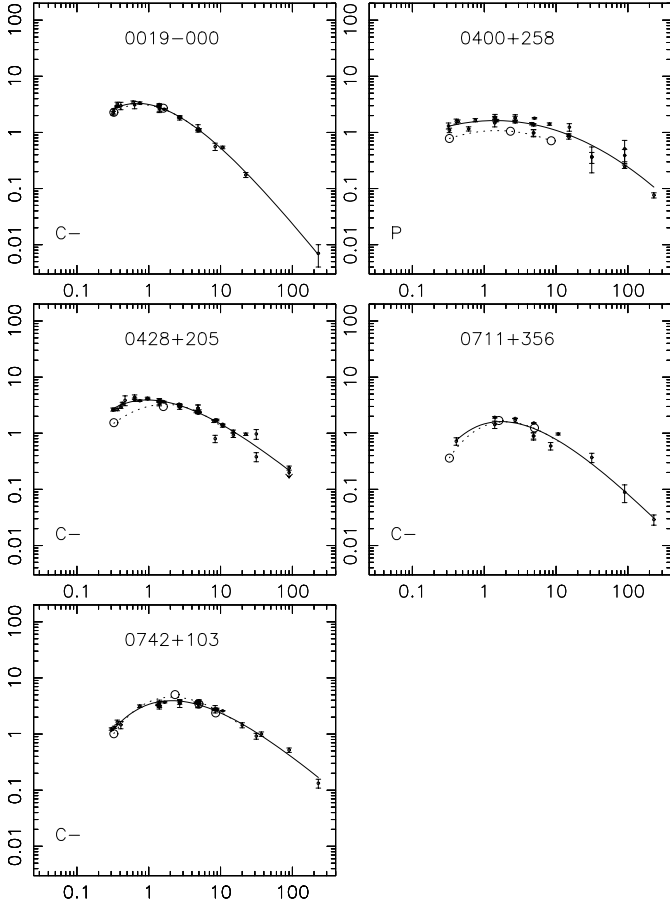


Fig. 5. The integrated spectra and the spectra of the dominant component from VLBI and IPS observations for GPS sources which have one dominant component. The x-axis is in units of GHz while the y-axis is in units of Jy. The filled circles and the continuous lines represent the integrated spectrum, while the VLBI and IPS flux densities of the dominant component are denoted by open circles. The dotted lines denote the fits to the spectra of the components using these measurements and the integrated flux densities at higher frequencies, except for 0428+205 where only the component flux densities have been fitted. The spectra have been fitted using the expressions $\log S = a_0 + a_1 \log \nu + a_2 (\log \nu)^2$ for 0428+205 which is marked P, and $\log S = a_0 + a_1 \log \nu + a_2 e^{-\log \nu}$ for the remaining four sources which are marked C-.

geometric mean of the major and minor axes. Column 8: the size of the IPS component in mas; Column 9: the expected size of the dominant component if the turnover is due to synchrotron self absorption. The angular size of the self absorbed component

can be estimated from (cf. Kellermann et al. 1981)

$$\theta \approx 13.45 \nu_p^{-5/4} S_p^{1/2} B^{1/4} (1+z)^{1/4}$$

where θ is in mas, peak frequency ν_p in GHz, the flux density at the peak frequency, S_p is in Jy and the magnetic field B in Gauss. We have assumed a redshift of 1 for the source 0742+103 Columns 10 and 11: the electron density of the absorbing medium, if the absorption is due to thermal free-free absorption. This is given by (cf. Osterbrock 1989)

$$n_e^2 \approx 3.05 \times 10^6 T^{1.35} \nu^{2.1} \left(\frac{1}{L}\right) \text{cm}^{-6}$$

where ν is in GHz, T is in units of 10^4 K and the size of the absorbing medium L in pc. We have assumed $T=10^4$ K and have listed the values of n_e for $L=10$ and 50 pc.

The expected size of the components if the turnover is due to synchrotron self absorption ranges from about 1 to 5 mas assuming a magnetic field of 10^{-4} Gauss (e.g. Mutel et al. 1985). The sizes and spectra of the components are generally consistent with synchrotron self absorption, although models involving free-free absorption are viable (cf. Bicknell et al. 1997). In the radio source 0400+258 the total linear separation of the components extends to over 10 mas (Fey & Charlot 1997), and could extend to larger sizes with the extended structure appearing somewhat diffuse, although the size of the individual components range from 0.3 – 2.8 mas. If the low-frequency turnover is due to free-free absorption the required densities of an absorbing medium of thickness 10 and 50 pc at a temperature of 10^4 K, are listed in Table 6. These values are in the range of 200 to 1200 cm^{-3} . Carvalho (1998) suggests that this dense gas might imply the frustration scenario where CSSs are as old as the larger FR II sources. However, estimates of this density could be reduced as in the model of Bicknell et al. (1997).

Recently Kuncic et al. (1998) considered the effect of induced compton scattering (ICS) by the external shell of thermal gas (Bicknell et al. 1997) to explain the low frequency turnover of the GPS sources. The Thomson optical depth (τ_T) of the ICS screen ranges from about 0.001 to 0.04 for the model parameters quoted in Kuncic et al. (1998). Using the peak frequency of the components (Table 6), we estimate the angular sizes of the components to be in range of about 1 to 8 mas for τ_T of 0.001 and 7 to 50 mas for τ_T of 0.04. These values are consistent with the component sizes listed in Table 6, making it difficult to distinguish unambiguously between the different processes responsible for the low-frequency turnover.

6. Concluding remarks

We have determined the small-scale structure of samples of CSS, GPS and larger sources at 327 MHz using the technique of IPS with the Ooty Radio Telescope. We have also compiled the information on the structure of these sources and summarise the conclusions based on both our IPS and interferometric measurements.

1. The prominence of the hotspots shows very little dependence on the luminosity of the radio source over few decades of luminosity from about $10^{25.5}$ to 10^{28} $\text{W Hz}^{-1} \text{sr}^{-1}$. The prominence of the hotspots also shows no significant dependence on the linear size over about two decades in linear size. These are based on both the IPS observations as well as interferometric observations from the literature.
2. The size of the hotspots were shown earlier to increase linearly with the projected linear size for the CSS and GPS sources upto about 20 kpc, and then flattens at larger distances by considering objects observed with a similar number of resolution elements (Jeyakumar & Saikia 2000a,b). The sizes of the hotspots estimated from the IPS observations as well as the interferometric observations of hotspots with resolutions comparable to the IPS cut-off size are consistent with this flattening.
3. We identify candidates for milliarcsec ‘halos’ at 327 MHz in 8 CSS and GPS objects. These could be due to earlier periods of activity or diffusion of relativistic electrons from the jets and lobes. VLBI imaging at low-frequencies of these sources would be useful to clarify the situation.
4. We have determined the spectra of the dominant component in five GPS objects from both IPS and VLBI observations in order to distinguish between free-free and synchrotron self absorption. The turnover in their spectra is consistent with synchrotron self absorption although models involving free-free absorption are viable.

Acknowledgements. We thank Divya Oberoi, and all the observers at Ooty, particularly Ravi Kumar, Magesh and Raghunathan, for their help during the observations, and Pradeep Gothoskar and P.K. Manoharan for numerous discussions to clarify the finer points of IPS. We thank an anonymous referee, Pradeep Gothoskar, V. K. Kulkarni and P. K. Manoharan for their valuable comments on the manuscript. We have made use of the NASA/IPAC Extragalactic Database, operated by the Jet Propulsion Laboratory, California Institute of Technology under contract with NASA.

References

- Akujor C.E., Garrington S. T., 1995, A&AS 112, 235
 Akujor C.E., Spencer R.E., Saikia D.J., 1991a, A&A 249, 337
 Akujor C.E., Spencer R.E., Zhang F.J., et al., 1991b, MNRAS 250, 215
 Akujor C.E., Spencer R.E., Zhang F.J., et al., 1993, A&A 274, 752
 Akujor C.E., Lüdke E., Browne I.W.A., et al., 1994, A&AS 105, 247
 Allington-Smith J.R., 1982, MNRAS 199, 611
 Altschuler D.R., Gurvits L.I., Alef W., et al., 1995, A&AS, 114, 197
 Appl S., 1996, In: Hardee P.E., Bridle A.H., Zensus J.A. (eds.) Energy Transport in Radio Galaxies and Quasars. ASP Conference Series Vol. 100, p. 129
 Appl S., Camenzind M., 1992, A&A 256, 354
 Appl S., Camenzind M., 1993a, A&A 270, 71
 Appl S., Camenzind M., 1993b, A&A 274, 699
 Barthel P.D., Miley G.K., 1988, Nat 333, 319
 Barthel P.D., Miley G.K., Schilizzi R.T., Lonsdale C.J., 1988, A&AS 73, 515
 Bedford N.H., Kerr A.J., Mathur S.H., et al., 1981, MNRAS 195, 245
 Begelman M.C. 1996, In: Carilli C.L., Harris D.E. (eds.) Cygnus A - study of a radio galaxy. Proc. Greenbank Workshop, p. 209
 Begelman M.C., Blandford R.D., Rees M.J., 1984, Rev. Mod. Phys. 56, 255
 Bicknell G.V., Dopita M.A., O’Dea C.P., 1997, ApJ 485, 112
 Blundell K.M., Rawlings S., Willott C.J., 1999, AJ 117, 677
 Bogers W., J., Hes R., Barthel P.D., Zensus J.A., 1994, A&AS 105, 91
 Bondi M., Padrielli L., Fanti R., et al., 1996, A&A 308, 415
 Bondi M., Garrett M.A., Gurvits L.I., 1998, MNRAS 297, 559
 Bridle A.H., Perley R.A., 1984, ARA&A 22, 319
 Bridle A.H., Hough D.H., Lonsdale C.J., Burns J.O., Laing R.A., 1994, AJ 108, 766 (B94)
 Broderick J.J., Condon J.J., 1975, ApJ 202, 596
 Carilli C.L., Wrobel J.M., Ulvestad J.S., 1998, AJ 115, 928
 Carvalho J.C., 1985, MNRAS 215, 463
 Carvalho J.C., 1994, A&A 292, 392
 Carvalho J.C., 1998, A&A 329, 845
 Cawthorne T.V., Scheuer P.A.G., Morison I., Muxlow T.W.B., 1986, MNRAS 219, 883
 Cawthorne T.V., Wardle J.F.C., Roberts D.H., Gabuzda D.C., 1993a, ApJ 416, 519
 Cawthorne T.V., Wardle J.F.C., Roberts D.H., Gabuzda D.C., Brown L.F., 1993b, ApJ 416, 496
 Cersosimo J.C., Santos M.L., Cintron S.I., Quiniento Z.M., 1994, ApJS 95, 157
 Charlot P., 1990, A&A 229, 51
 Chyzy K.T., 1997, MNRAS 289, 355
 Cohen M.H., Gundermann E.J., Harris D.E., 1967, ApJ 150, 767
 Cotton W.D., 1983, ApJ 271, 51
 Cotton W.D., Owen F.N., Geldzahler B.J., et al., 1984, ApJ 277, L41
 Cotton W.D., Owen F.N., Mahoney M.J., 1989, ApJ 338, 37
 Dallacasa D., Fanti C., Fanti R., Schilizzi R.T., Spencer R.E., 1995, A&A 295, 27
 Dallacasa D., Bondi M., Alef W., Mantovani F., 1998, A&AS 129,219
 Duffett-Smith P.J., 1980, MNRAS 192, 33
 Fanti C., Fanti R., Formigini L., Lari C., Padrielli L., 1977, A&AS 28, 351
 Fanti C., Fanti R., Parma P., Schilizzi R.T., van Breugel W.J.M., 1985, A&A 143, 292
 Fanti C., Fanti R., Parma P., et al., 1989, A&A 217, 44
 Fanti R., Fanti C., Schilizzi R.T., et al., 1990, A&A 231, 333
 Fanti C., Fanti R., Dallacasa D., et al., 1995, A&A 302, 317
 Fernini I., Burns J.O., Bridle A.H., Perley R.A., 1993, AJ 105, 1690
 Fernini I., Burns J.O., Perley R.A., 1997, AJ 114, 2292 (F97)
 Fey A.L., Clegg A.W., Fomalont E.B., 1996, ApJS 105, 299
 Fey A.L., Charlot P., 1997, ApJS 111, 95
 Frey S., Gurvits L.I., Kellermann K.I., Schilizzi R.T., Pauliny-Toth I.I.K., 1997, A&A 325, 511
 Gopal-Krishna, Patnaik A.R., Steppe H., 1983, A&A 123 107
 Gothoskar P., Rao A.P., 1999, Solar Phys. 185, 361
 Gregorini L., Padrielli L., Parma P., Gilmore G., 1988, A&AS 74, 107
 Gurvits L.I., Schilizzi R.T., Barthel P.D., et al., 1994, A&A 291, 737
 Hardcastle M.J., Alexander P., Pooley G.G., Riley J.M., 1998, MNRAS 296, 445

- Hewish A., Readhead A.C.S., 1976, *App. Lett.* 18, 1
- Hintzen P., Ulvested J., Owen F., 1983, *AJ* 88, 709
- Hodges M.W., Mutel R.L., Phillips R.B., 1984, *AJ* 89, 1327
- Jackson N., Roland J., Bremer M., Rhee G., Webb J., 1999, *A&AS* 134, 401
- Jenkins C., McEllin M., 1977, *MNRAS* 180, 219
- Jenkins C.J., Pooley G.G., Riley J.M., 1977, *Mem. R. Astron. Soc.* 84, 61
- Jeyakumar S., Saikia D.J., 2000a, *MNRAS* 311, 397
- Jeyakumar S., Saikia D.J., 2000b, In: Biretta J., et al. (eds.) *STScI workshop on Life Cycles of Radio Galaxies*. *New Astronomy Reviews* (in press)
- Jones T.W., Ryu D., Engel A., 1999a, *ApJ* 512, 105
- Jones T.W., Tregillis I.L., Ryu D., 1999b, In: Biretta J., et al. (eds.) *STScI workshop on Life Cycles of Radio Galaxies*. *New Astronomy Reviews* (in press)
- Kaiser C.R., Dennett-Thorpe J., Alexander P., 1997, *MNRAS* 292, 723
- Kapahi V.K., 1978, *A&A* 67, 157
- Kellermann K.I., Pauliny-Toth I.I.K., 1981, *ARA&A* 19, 373
- Kuncic Z., Bicknell G.V., Dopita M.A., 1998, *ApJ* 495, L35
- Laing R.A., 1989, In: Meisenheimer K., Roser H.J. (eds.) *Hot Spots in Extragalactic Radio Sources*. Springer-Verlag, p. 27
- Little L.T., Hewish A., 1966, *MNRAS* 134, 221
- Little L.T., Hewish A., 1968, *MNRAS* 138, 393
- Lonsdale C.J., Barthel P.D., Miley G.K., 1993, *ApJS* 87, 63
- Manoharan P.K., 1993, *Solar Phys.* 148, 153
- Manoharan P.K., 1997, *Geophys. Res. Lett.* 24, 2623
- Manoharan P.K., Ananthakrishnan S., 1990, *MNRAS* 244, 691
- Manoharan P.K., Kojima M., Misawa H., 1994, *J. Geophys. Res.* 99, 23411
- Mantovani F., Muxlow T., Padrielli L., 1988, In: Reid M.J., Moran J.M. (eds.) *The Impact of VLBI on Astrophysics and Geophysics*. *IAU Symp.* 129, p. 125
- Mantovani F., Saikia D.J., Browne I.W.A., et al., 1990, *MNRAS* 245, 427
- Mantovani F., Junor W., Fanti R., et al., 1992, *MNRAS* 257, 353
- Mantovani F., Junor W., Fanti R., Padrielli L., Saikia D.J., 1994a, *A&A* 292, 59
- Mantovani F., Junor W., Bondi M., 1994b, In: Zensus J.A., Kellermann K.I., (eds.) *Compact extragalactic Radio sources.. NRAO-Workshop 23*, p. 29
- Mantovani F., Bondi M., Junor W., Salter C.J., Saikia D.J., 1998, In: Zensus J.A., Taylor G.B., Wrobel J.M. (eds.) *Radio Emission from Galactic and Extragalactic Compact Sources*. *ASP Conference Series*, Vol. 144, p. 299
- Miley G.K., Hartsuijker A.P., 1978, *A&AS* 34, 129
- Murphy D.W., Browne I.W.A., Perley R.A., 1993, *MNRAS* 264, 298
- Mutel R.L., Hodges M.W., 1986, *ApJ* 307, 472
- Mutel R.L., Phillips R.B., 1988, In: Reid M.J., Moran J.M. (eds.) *The Impact of VLBI on Astrophysics and Geophysics*. *IAU Symp.* 129, p. 73
- Mutel R.L., Hodges M.W., Phillips R.B., 1985 *ApJ* 290, 86
- Neff S.G., Hutchings J.B., Gower A.C., 1989, *AJ* 97, 1291
- Neff S.G., Roberts L., Hutchings J.B., 1995, *ApJS* 99, 349
- Norman M.L., 1996, In: Hardee P.E., Bridle A.H., Zensus J.A. (eds.) *Energy Transport in Radio Galaxies and Quasars*. *ASP Conference Series* Vol. 100, p. 319
- Norman M.L., Balsara D.S., 1993, In: Meisenheimer K., Roeser H.-J. (eds.) *Jets in Extragalactic Radio Sources*. Springer Verlag, p. 229
- O'Dea C.P., 1998, *PASP* 110, 493
- O'Dea C.P., Baum S.A., 1997, *AJ* 113, 148
- O'Dea C.P., Baum S.A., Stanghellini C., 1991, *ApJ* 380, 66
- O'Dea C.P., Baum S. A., Stanghellini C., et al., 1992, *AJ* 104, 1320
- Osterbrock D.E., 1989, *Astrophysics of Gaseous Nebulae and Active Galactic Nuclei*. University Science Books, Mill Valley
- Padrielli L., Eastman W., Gregorini L., Mantovani F., Spangler S., 1991, *A&A* 249, 351
- Patnaik A.R., Porcas R.W., Browne I.W.A., 1995, *MNRAS* 274, L5
- Peacock J.A., Wall J.V., 1982, *MNRAS* 198, 843
- Pearson T.J., Readhead A.C.S., 1988, *ApJ* 328, 114
- Pearson T.J., Readhead A.C.S., Wilkinson P.N., 1980, *ApJ* 236, 714
- Pearson T.J., Perley R.A., Readhead A.C.S., 1985, *AJ* 90, 738
- Perley R.A., 1982, *AJ* 87, 859
- Perley R.A., 1989, In: Meisenheimer K., Roser H.J. (eds.) *Hot Spots in Extragalactic Radio Sources*. Springer-Verlag, p. 1
- Phillips R.B., Mutel R.L., 1981, *ApJ* 244, 19
- Polatidis A.G., Wilkinson P.N., Xu W., et al., 1995, *ApJS* 98, 1
- Preston R.A., Jauncey D., Meier D.L., et al., 1989, *AJ* 98, 1
- Price R., Gower A.C., Hutchings J.B., et al., 1993, *ApJS* 86, 365
- Rantakyrö F.T., Bååth L.B., Dallacasa D., Jones D.L., Wehrle A.E., 1996, *A&A* 310, 66
- Rao A.P., Bhandari S.M., Ananthakrishnan S., 1974, *Aust. J. Phys.* 27, 105
- Readhead A.C.S., Taylor G.B., Xu W., et al., 1996a, *ApJ* 460, 612
- Readhead A.C.S., Taylor G.B., Pearson T.J., Wilkinson P.N., 1996b, *ApJ* 460, 634
- Rendong N., Schilizzi R.T., Fanti C., Fanti R., 1991, *A&A* 252, 513
- Romney J., Padrielli L., Bartel N., et al., 1984, *A&A* 135, 289
- Saikia D.J., Shastri P., Kapahi V.K., Sinha R.P., Swarup G., 1984, *JA&A* 5, 429
- Saikia D.J., Shastri P., Cornwell T.J., Junor W., Muxlow T.W.B., 1989, *JA&A* 10, 203
- Saikia D.J., Holmes G.F., Kulkarni A.R., Salter C.J., Garrington S.T., 1998, *MNRAS* 298, 877
- Sanders R.H., 1983, *ApJ* 266, 73
- Sanghera H.S., Saikia D.J., Lúdice E., et al., 1995, *A&A* 295, 629
- Savage A., Jauncey D.L., White G.L., et al., 1990, *Aust. J. Phys.* 43, 241
- Scheuer P.A.G., 1982, In: Heeschen D.S., Wade C.M. (eds.) *IAU Symp.* 97, *Extragalactic Radio Sources*. Reidel, Dordrecht, p. 163
- Schilizzi R.T., Kapahi V.K., Neff S.G., 1982, *JA&A* 3, 173
- Shaw M.A., Tzioumis A.K., Pedlar A., 1992, *MNRAS* 256, 6p
- Silver C.S., Taylor G.B., Vermeulen R.C., 1998, *ApJ* 502, 229
- Smith M.D., Norman M.L., Winkler K.-H.A., Smarr L., 1985, *MNRAS* 214, 67
- Spencer R.E., McDowell J.C., Charlesworth M., et al., 1989, *MNRAS* 240, 657
- Spencer R.E., Schilizzi R.T., Fanti C., et al., 1991, *MNRAS* 250, 225
- Spoelstra T.A.T., Patnaik A.R., Gopal-Krishna, 1985, *A&A* 152, 38
- Stanghellini C., Baum S.A., O'Dea C.P., Morris G.B., 1990, *A&A* 233, 379
- Stanghellini C., O'Dea C.P., Baum S.A., et al., 1997, *A&A* 325, 943
- Stanghellini C., O'Dea C.P., Dallacasa D., et al., 1998a, *A&AS* 131, 303
- Stanghellini C., Dallacasa D., O'Dea C.P., et al., 1998b, In: Zensus J.A., Taylor G.B., Wrobel J.M. (eds.) *IAU Colloquium 164, Radio Emission from Galactic and Extragalactic Compact Sources*. *ASP Conference Series* Vol. 144, p. 177
- Stanghellini C., O'Dea C.P., Murphy D.W., 1999, *A&AS* 134, 309
- Steppe H., Jeyakumar S., Saikia D.J., Salter C.J., 1995, *A&AS* 113, 409
- Strom R.G., Riley J.M., Spinard H., et al., 1990 *A&A* 227, 19

- Taylor G.B., Vermeulen R.C., Pearson T.J., et al., 1994, *ApJS* 95, 345
- Tregillis I.L., Jones T.W., Ryu D., Park C., 1999, In: Biretta J., et al. (eds.) STScI workshop, *Life Cycles of Radio Galaxies*. New Astronomy Reviews (in press)
- van Breugel W., Miley G., Heckman T., 1984, *AJ* 89, 5
- van Breugel W.J.M., Fanti C., Fanti R., et al., 1992, *A&A* 256, 56
- Venugopal V.R., Ananthakrishnan S., Swarup G., Pynzar A.V., Udaltsov V.A., 1985, *MNRAS* 215, 685
- Wardle J.F.C., Moore R.L., Angel J.R.P., 1984, *ApJ* 279, 93
- Wehrle A.E., Cohen M.H., Unwin S.C., et al., 1992, *ApJ* 391, 589
- Wilkinson P.N., Spencer R.E., Readhead A.C.S., Pearson T.J., Simon R.S., 1984, In: Fanti R., Kellermann K.I., Setti G. (eds.) *IAU Symp. 110, VLBI and Compact Radio Sources*. p. 25
- Wilkinson P.N., Tzioumis A.K., Benson J.M., et al., 1991a, *Nat* 352, 313
- Wilkinson P.N., Akujor C.E., Cornwell T.J., Saikia D.J., 1991b, *MNRAS* 248, 86
- Wilson M.J., Falle S.A.E.G., 1985, In: Kahn F.D. (eds.) *Cosmical Gas Dynamics*. VNU Science Press, p. 259
- Wilson M.J., Scheuer P.A.G., 1983, *MNRAS* 205, 449